

Materials Advances

Accepted Manuscript

This article can be cited before page numbers have been issued, to do this please use: M. Fatahi, D. Chen and E. Zysman-Colman, *Mater. Adv.*, 2025, DOI: 10.1039/D5MA00586H.



This is an Accepted Manuscript, which has been through the Royal Society of Chemistry peer review process and has been accepted for publication.

Accepted Manuscripts are published online shortly after acceptance, before technical editing, formatting and proof reading. Using this free service, authors can make their results available to the community, in citable form, before we publish the edited article. We will replace this Accepted Manuscript with the edited and formatted Advance Article as soon as it is available.

You can find more information about Accepted Manuscripts in the [Information for Authors](#).

Please note that technical editing may introduce minor changes to the text and/or graphics, which may alter content. The journal's standard [Terms & Conditions](#) and the [Ethical guidelines](#) still apply. In no event shall the Royal Society of Chemistry be held responsible for any errors or omissions in this Accepted Manuscript or any consequences arising from the use of any information it contains.



University
of
St Andrews

ELI ZYSMAN-COLMAN, Ph.D., FRSC Article Online
DOI: 10.1039/D5MA00586H

**Organic Semiconductor Centre
EaStCHEM School of Chemistry, University of St Andrews,
Purdie Building, North Haugh
KY16 9ST**

eli.zysman-colman@st-andrews.ac.uk
Tel.: +44-1334 463826; Fax.: +44-1334 463808
<http://www.zysman-colman.com>

17/04/2025

Data Availability Statement

The research data supporting this publication can be accessed at <https://doi.org/10.17630/e4521ae2-e1ea-45c2-8f60-880c6d12e8a6>. This link will be made active upon acceptance of the manuscript.

Sincerely,

Eli Zysman-Colman on behalf of the co-authors
Professor of Optoelectronic Materials



Blue Emission in Sterically Shielded Multiresonant Thermally Activated Delayed Fluorescence Emitters

Mahni Fatahi^{a‡}, Dongyang Chen^{a,b‡} and Eli Zysman-Colman^{*a}

^aOrganic Semiconductor Centre, EaStCHEM School of Chemistry, University of St Andrews, St Andrews, UK, KY16 9ST. E-mail: eli.zysman-colman@st-andrews.ac.uk

^bInstitute of Functional Nano & Soft Materials (FUNSOM), Soochow University, Suzhou, 21523, Jiangsu, PR China

[‡] These authors contributed equally

Keywords: TADF, OLED, Hyperfluorescence, Multiresonant TADF, Blue emitter

Abstract

Multiresonant TADF materials are a promising class of emitters capable of addressing the BT.2020 industry requirement for blue emission in electroluminescent displays as they simultaneously show narrowband emission and can harvest both singlet and triplet excitons to produce light. However, these emitters are typically planar and prone to aggregation and their moderately large singlet-triplet energy gap (ΔE_{ST}) leads to slow upconversion kinetics resulting in severe efficiency roll-off in the device. In this study we present a molecular design that simultaneously results in an emitter having a faster reverse intersystem crossing rate constant (k_{RISC}) and suppressed aggregation in the film state. **Mes-*r*DABNA** emits at λ_{PL} of 465 nm as 4 wt% doped films in SF3-RZ and has a short delayed lifetime of 45.2 μ s. Vacuum-deposited OLEDs with **Mes-*r*DABNA** showed blue emission at CIE coordinates of (0.13, 0.15) and a maximum external quantum efficiency, EQE_{max} , of 18.4%. Unsurprisingly, these devices suffered from rather strong efficiency roll-off (EQE_{1000} of 5.6%). With the aim of addressing this efficiency roll-off, hyperfluorescent devices containing **DMAC-DPS** as a TADF sensitizer were fabricated, which showed an improved EQE_{max} of 23.1% at CIE coordinates of (0.13, 0.17) and milder efficiency roll-off (EQE_{1000} of 12.7%). These devices showed one of the highest EQE_{1000} based on DABNA-based emitters to date.

Introduction

In recent years, thermally activated delayed fluorescence (TADF) emitters have emerged as one of the most promising emitter materials for organic light-emitting diodes (OLEDs). This is because of their excellent exciton harvesting properties that rival those of phosphorescent materials. TADF emitters are capable of harvesting up to 100% of the electrically generated excitons due to their small energy gap between the lowest excited singlet (S_1) and triplet excited states (T_1), ΔE_{ST} .¹ A subclass of TADF compounds, multi-resonant TADF (MR-TADF) emitters, produces desirable, bright, narrowband emission associated with high photoluminescence quantum yields ($\Phi_{PL} > 90\%$) and narrow full-width half maxima (FWHM < 50 nm). MR-TADF emitters are typically *p*- and *n*-doped polycyclic aromatic hydrocarbons (PAHs) having low-lying excited states possessing short-range charge transfer (SRCT) character.²⁻⁷ A key challenge in emitter design, including for multi-resonant TADF (MR-TADF) emitters, is achieving the blue Commission Internationale de l'Éclairage (CIE) coordinates of (0.131, 0.046) specified by the BT.2020 standard for pure blue emission.



However, the planar structure of most MR-TADF emitter cores makes them prone to aggregation, leading to red-shifted and broadened emission spectra, as well as aggregation-caused quenching (ACQ), all of which are detracting features that adversely affect the color and Φ_{PL} of blue MR-TADF emitters. For example, the first reported MR-TADF emitter, **DABNA-1** (Figure 1

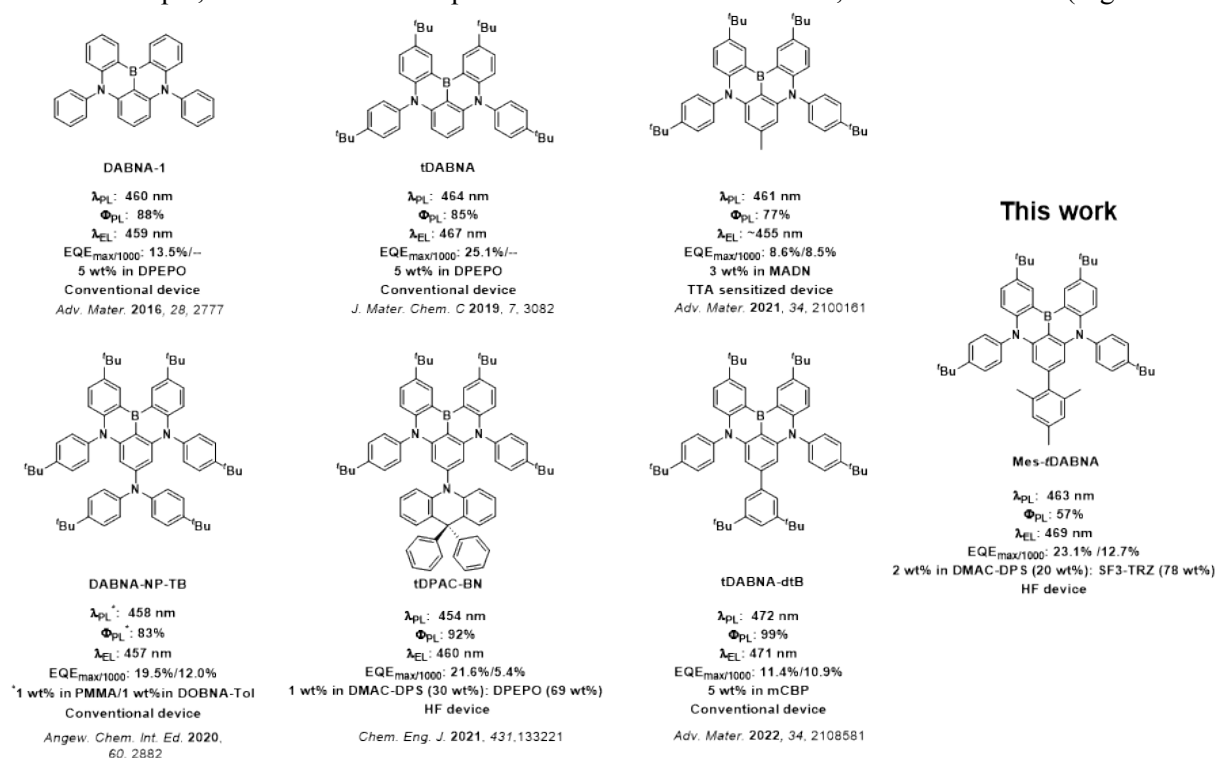


Figure 1), emits at λ_{PL} at 460 nm (FWHM = 28 nm) and has a Φ_{PL} of 88% in 1 wt% doped films in mCBP.⁸ However, Lee *et al.* disclosed that serious ACQ occurred when concentrations of greater than 5 wt% of **DABNA-1** were used in doped films,⁹ and peripheral bulky groups like *tert*-butyl moieties can mitigate it. The derivative **t-DABNA** (Figure 1) maintains a high Φ_{PL} of 85%, and blue λ_{PL} of 464 nm at 5 wt% doping in DPEPO film. The OLEDs with 5 wt% **t-DABNA** in DPEPO showed a higher $E_{QE_{max}}$ of 25.1% at λ_{EL} of 467 nm and CIE coordinates of (0.13, 0.15) compared to the device with 5 wt% **DABNA-1** in mCBP ($E_{QE_{max}}$ = 12.5%; λ_{EL} of 461 nm, CIE coordinates of (0.13, 0.10)).⁸ However, both devices still suffered from severe efficiency roll-off and the device did not even reach a luminance of 1000 cd m⁻².⁹ There have since been a number of studies focussing on addressing this issue by decorating the **tDABNA** core with different bulky moieties. For instance, **tDABNA-dtB**,¹⁰ **DABNA-NP-TB** (also published as **3tPAB** and **t-DAB-DPA**),¹¹⁻¹³ **tDPAC-BN**¹⁴ and **M-tDABNA**¹⁵ are all examples with bulky substituents at the *para* position to the boron on the central phenyl ring (Figure 1). The **DABNA** derivatives containing an electron-donating group show blue-shifted emission at λ_{PL} of 461, 458, and 454 nm for **M-tDABNA** (3 wt% mCBP), **DABNA-NP-TB** (3 wt% mCP) and **tDPAC-BN** (1 wt%:30 wt% DMAC-DPS: DPEPO), respectively, compared to **tDABNA** (466 nm, 3 wt% mCBP). Whereas **t-DABNA-dtB**, contains uses di-*tert*-butylphenyl substituent, shows a red-shifted emission to 472 nm (5 wt% mCBP), compared to **tDABNA** (466 nm, 3 wt% mCBP), this red shift can be explained by the larger conjugated system in this molecule. The device with 5 wt% **t-DABNA-dtB** showed a rather low $E_{QE_{max}}$ of 11.4% but also low efficiency roll-off, reflected in an $E_{QE_{1000}}$ of 10.9%. The lower $E_{QE_{max}}$ is due to the choice of device stack that is optimised for device lifetime rather than high EQE (LT₉₅=205 h). The CIE coordinates of the device of (CIE 0.11, 0.14) are similar to those of devices with **DABNA-1**. The OLED with the donor-extended derivative **tDPAC-BN** showed an $E_{QE_{max}}$ of 21.6% at CIE coordinates of (0.14, 0.09). Similar to the devices with the aforementioned derivatives as emitters, that with **tDPAC-BN** showed a reduced efficiency roll-off and the $E_{QE_{1000}}$ was



5.4%. Devices reported by Kim *et al.* employing **DABNA-NP-TB (t-DAB-DPA)** as the emitter showed a higher EQE_{max} of 27.9% [CIE coordinates of (0.13, 0.08)] as compared to that with **tDABNA** [23.9%; CIE coordinates of (0.13, 0.10)] accompanied by a less severe efficiency roll-off (EQE_{1000} of 8.1% as compared to 3.4% for the device with **tDABNA**).¹¹ This consistently improved performance of the OLEDs employing **tDABNA** derivatives as emitters compared to devices with the parent can be correlated to two factors: one is the reduced ACQ and second is the faster k_{RISC} of $3.97 \times 10^4 \text{ s}^{-1}$ for **DABNA-NP-TB (t-DAB-DPA)** (3 wt% in mCBP:mCBPCN) versus $1.17 \times 10^4 \text{ s}^{-1}$ for **tDABNA** (3 wt% in mCBP:mCBPCN)¹¹, which reduces the likelihood of triplet quenching processes.

From these examples, a correlation between reduced efficiency roll-off and mitigated ACQ can be drawn. As previously reported by some of us, the introduction of mesityl groups onto planar MR-TADF cores can effectively reduce ACQ. One example is the decoration of three mesityl groups about the carbonyl/nitrogen based core **DiKTa** (QAO).¹⁶ The OLEDs with **Mes₃DiKTa** showed an EQE_{max} of 21.1% and an EQE_{100} of 14.5%, which represents an improved performance as compared to the device with **DiKTa** ($\text{EQE}_{\text{max}} = 14.7\%$; $\text{EQE}_{100} = 8.5\%$).¹⁷

In this study, we present a novel blue MR-TADF emitter, **Mes-tDABNA** (Figure 1) that conserves the blue emission of the **tDABNA** core while simultaneously mitigating aggregation and alleviating efficiency roll-off in vacuum-deposited OLEDs. This is achieved by incorporating a mesityl group at the *para* position to the boron atom, which in contrast to the 3,5-di-*tert*-butyl-phenyl group used in **t-DABNA-dtB** does not increase the conjugation length and only serves as a steric blocking group. Theoretical calculations predict a small ΔE_{ST} of 160 meV and low-lying SRCT excited states. In toluene solution, **Mes-tDABNA** shows narrowband blue emission at λ_{PL} of 460 nm (FWHM of 25 nm). The emission is red-shifted to 464 nm and broadened (FWHM of 39 nm) as a 4 wt% doped film in SF3-TRZ. In these films, **Mes-tDABNA** has a prompt lifetime, $\tau_{\text{p,avg}}$ of 13.4 ns, and a delayed emission lifetime, $\tau_{\text{d,avg}}$ of 45 μs . This leads to a relatively faster k_{RISC} of $5.53 \times 10^4 \text{ s}^{-1}$ as compared to **tDABNA** ($k_{\text{RISC}} = 2.44 \times 10^3 \text{ s}^{-1}$; 5 wt% doped films in DPEPO)⁹ The OLEDs showed an EQE_{max} of 18.4% and a maximum luminance (L_{max}) of 3600 cd m^{-2} . Unfortunately, these devices showed a strong efficiency roll-off (EQE_{1000} of 5.6%), so we explored a hyperfluorescent (HF) device structure to enhance the device performance. The HF devices showed an improved EQE_{max} of 23.1% and a milder efficiency roll-off (EQE_{1000} of 12.7%). The maximum luminance was also more than doubled to 8400 cd m^{-2} .



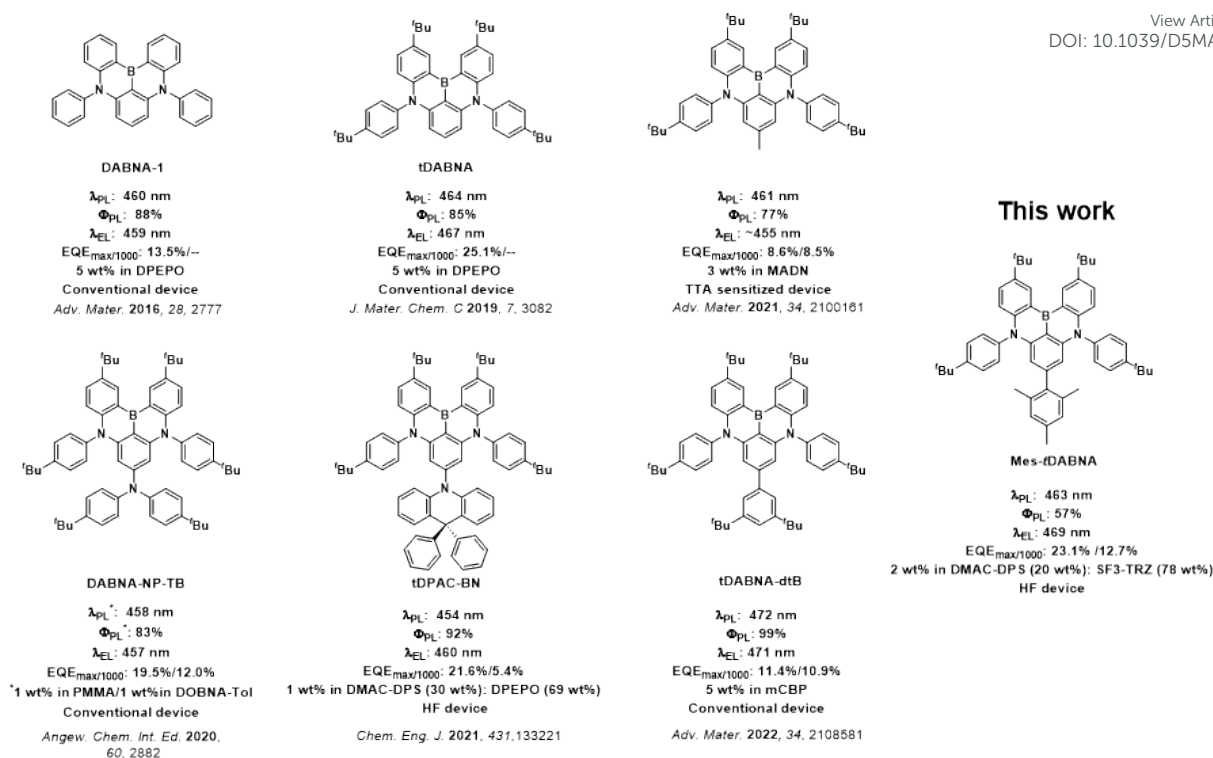


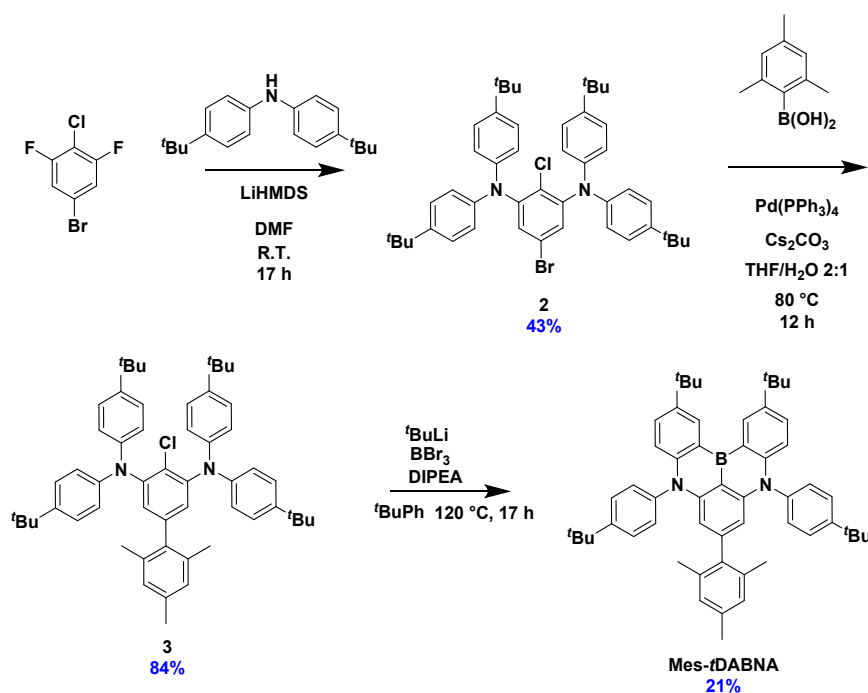
Figure 1. Chemical structures, photophysical properties and device performance of **Mes-tDABNA** and examples of tDABNA derivatives in literature.¹⁰⁻¹⁵

Results and Discussion

Synthesis and Characterisation

The synthesis was carried out as shown in Scheme 1. Nucleophilic aromatic substitution of bis(di-*tert*-butyl)amine with bromo-4-chloro-3,5-difluorobenzene gave **2** in 43% yield. The mesityl group was installed *via* a Suzuki-Miyaura cross-coupling between mesitylboronic acid and **2** in 84% yield. Compound **3** was subjected to a tandem lithiation and borylation protocol⁸ to afford **Mes-tDABNA** in a 21% yield, which is somewhat lower compared to those reported for **DABNA-1** (32%)⁸ and **tDABNA** (31%)⁹ but similar to that reported for **M-tDABNA** (27%)¹⁵. The identity and purity of **Mes-tDABNA** and the intermediates were determined using melting point (Mp) analysis, ¹H and ¹³C nuclear magnetic resonance (NMR) spectroscopy, high-resolution mass spectrometry (HRMS), high performance liquid chromatography (HPLC) and elemental analysis. Thermal gravimetric analysis (TGA) and Mp determination revealed that **Mes-tDABNA** has a high melting point of 300-304 °C and degradation temperature, *T_d* (at 5% weight loss) of 363 °C (Figure S3), the latter of which is lower compared to that of **tDABNA** (419 °C)⁹.



Scheme 1. Synthesis of **Mes-tDABNA**.

Theoretical calculations

The optimized ground-state geometry and electronic structure of **Mes-tDABNA** were calculated using density functional theory (DFT) at the PBE0/6-31G(d,p) level in the gas phase.¹⁸ The HOMO is localized on the central benzene and one half of each of the amine donor moieties that is conjugated to it. Due to the symmetry of the compound, there is no electron density on either the boron atom or the *ipso* or *para* carbons to it of the central aryl ring. The electron density of the LUMO is distributed over the same skeleton as the HOMO but with significant density on boron and also the carbon centres *ipso* and *para* to it. The calculated HOMO/LUMO energy levels are -4.82/-0.94 eV. Both the HOMO and LUMO are stabilized compared to those of **M-tDABNA** (-4.79/-0.88 eV) (Figure S1), which is due to the weakly inductively electron-withdrawing character of the mesityl group.

The spin-orbit coupling matrix element (SOCME) between S_1 and T_1 state at the T_1 optimized geometry calculated at the TDA-DFT-PBE0/6-31G(d,p) level of theory is not unusually small at 0.06 cm^{-1} .¹⁹ The excited-state energies were calculated at the spin-component scaling second-order algebraic diagrammatic construction (SCS-(ADC)2/cc-pVDZ) level, as this level of theory has been shown to predict accurately the ΔE_{ST} of MR-TADF compounds.²⁰ The energy for the first excited singlet (S_1) and triplet (T_1) states are 2.91 and 2.75 eV, respectively, leading to a moderately small energy gap between (ΔE_{ST}) of 0.16 eV. Compared to **M-tDABNA** (3.15/3.03 eV), both the S_1 and T_1 states are stabilized while the ΔE_{ST} is larger by 40 meV. The difference density plots of the S_1 and T_1 states are shown in Figure 2 (Figure S1 for **M-tDABNA**). Their patterns indicate that both of these states possess SRCT character. The S_0 - S_1 transition has a calculated oscillator strength, f , of 0.24, which is lower than the corresponding transition in **M-tDABNA** (0.28).



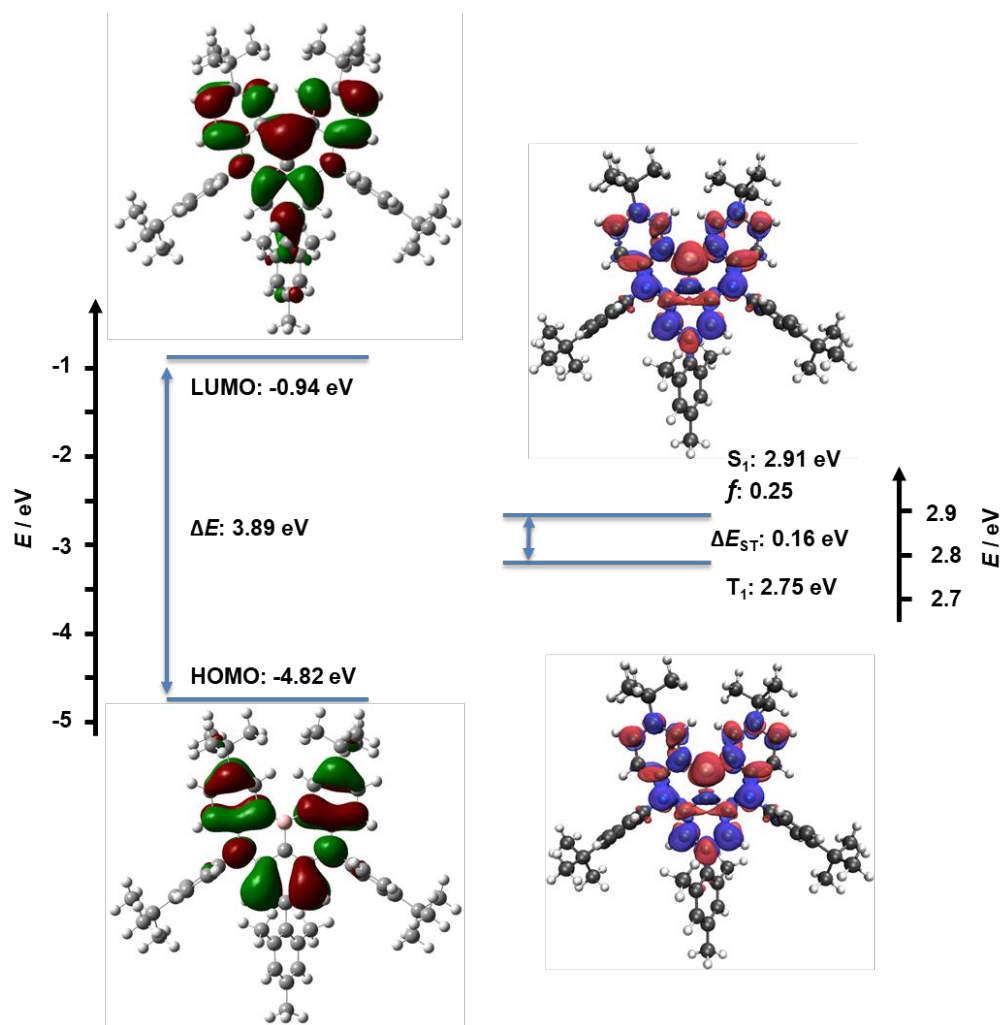


Figure 2. Calculated HOMO and LUMO energies and the electron density plots calculated at the PBE0/6-31G(d,p) level in the gas phase and calculated excited-state energies and the corresponding different density plots for hole and electron for the S_1 and T_1 states at the SCS-ADC(2)/cc-pVDZ level in the gas phase (blue: negative, red: positive, isovalue: 0.02).

Photophysical properties

The absorption and steady-state photoluminescence (PL) spectra in dilute toluene ($\times 10^{-5}$ M) are shown in Figure 3. The absorption spectrum of **Mes-tDABNA** shows an intense lowest energy band at 444 nm with a molar extinction coefficient (ϵ) of $24 \times 10^3 \text{ M}^{-1} \text{ cm}^{-1}$. This band is associated with the SRCT transition and is essentially isoenergetic and isoabsorptive as that of **tDABNA** (444 nm, $21 \times 10^3 \text{ M}^{-1} \text{ cm}^{-1}$).²¹ The PL spectrum is narrowband with a peak maximum, λ_{PL} , of 460 nm and a full-width at half maximum (FWHM) of 25 nm. This is effectively the same as that of **tDABNA** (λ_{PL} of 457 nm and FWHM of 26 nm in toluene).¹⁰ The small Stokes shift of 16 nm is associated with the rigid structure and the small degree of geometric reorganization in the excited state of this compound. The photoluminescence quantum yield, Φ_{PL} , is 75%, which decreases to 54% under aerated conditions. The time-resolved photoluminescence measurements revealed monoexponential decay kinetics, with a prompt lifetime, τ_{p} , of 7.9 ns, while no delayed emission was observed for both **tDABNA** and **M-tDABNA**, and no solution Φ_{PL} or lifetime are reported in the literature. The S_1 and T_1 levels were determined from the onsets of the steady-state and time-gated PL spectra in dilute 2-methyltetrahydrofuran (2-MeTHF) glass at 77 K (Figure 3). The S_1 is 2.78 eV and the T_1 is 2.65 eV, resulting in a ΔE_{ST} of 130 meV, all of which are in good agreement with those predicted by the SCS-ADC(2) calculations ($S_1=2.91$ eV; $T_1=2.75$ eV; $\Delta E_{\text{ST}}=0.16$ eV), and is smaller than those reported for **tDABNA** (2.82/2.62 eV, $\Delta E_{\text{ST}}=200$ meV in toluene/ frozen THF).¹⁰ Compared to **M-tDABNA** (ΔE_{ST}



= 110 meV in toluene)¹⁵ the ΔE_{ST} is larger by 20 meV, which again is in good agreement with the trend predicted by the SCS-ADC(2) calculations (Figure 2 and S1).

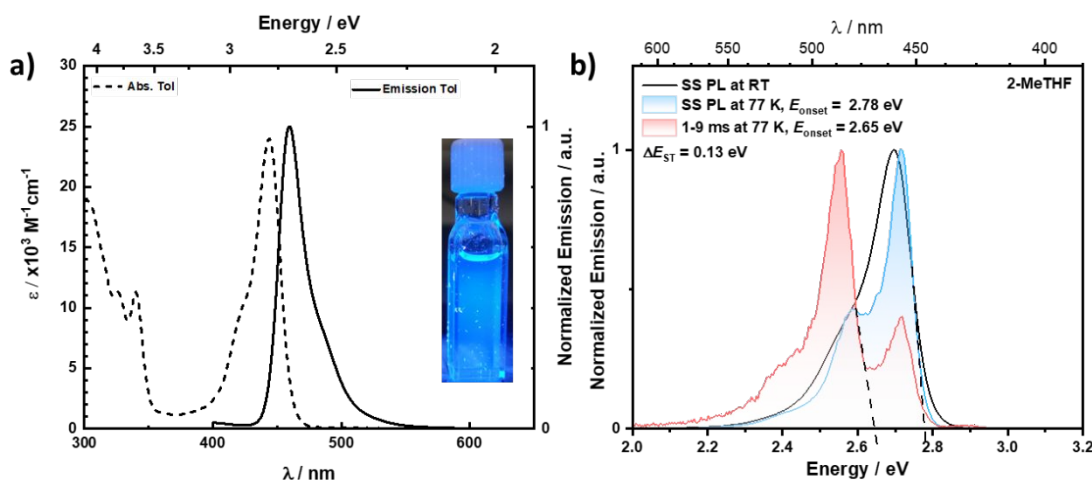


Figure 3. Absorption and PL spectra of dilute solutions of **Mes-tDABNA**; (a) absorption (dashed) and PL spectra (solid) of **Mes-tDABNA** in dilute ($\times 10^{-5}$ M) toluene solution ($\lambda_{exc} = 340$ nm); (b) Steady-state PL spectra of **Mes-tDABNA** in dilute 2-MeTHF solution/glass at room temperature (black) and 77 K (blue), time gated (1-9 ms) PL spectrum of **Mes-tDABNA** in 2-MeTHF glass (red) ($\lambda_{exc} = 340$ nm).

The *n*-typed material **SF3-TRZ** was chosen as the host for our emitter due to its suitably high T_1 energy (2.80 eV) and balanced carrier transporting abilities.^{5, 22} Excitation at 340 nm into the host of the 4 wt% doped film resulted in efficient Förster resonance energy transfer (FRET) and a Φ_{PL} of 58% (Figure S6); in air the Φ_{PL} decreases to 20%. In this film **Mes-tDABNA** emits at λ_{PL} of 464 nm, with a slightly broader envelope (FWHM of 39 nm), which may indicate that aggregates in the solid state contribute to the emission profile. (Figure 4). The time-resolved PL measurements using time correlated single photon counting (TCSPC) revealed an average $\tau_{p,avg}$ of 13.4 ns (fitted using a multiexponential decay function) and a long emission tail. This delayed emission decay was measured using multichannel scaling (MCS), with an average delayed emission lifetime, $\tau_{d,avg}$, of 45.2 μ s. Temperature-dependent time-resolved PL measurements revealed a very weak temperature dependence of the prompt fluorescence decay and a strong temperature dependence of the delayed fluorescence decay, the latter of which confirmed the TADF character of this compound (Figure 4 and Figure S8). Additionally, the temperature-dependent PL spectra revealed the emergence of a second emission band at λ_{PL} of 491 nm as the temperature decreased below 150 K, which can be ascribed to phosphorescence (Figure S9). A ΔE_{ST} of 140 meV was determined from the difference in the onsets of the steady-state PL and the phosphorescence spectra at 77 K. The corresponding S_1 (2.78 eV) and T_1 (2.64 eV) state energies coincide with those measured in 2-MeTHF glass. The rate constants for radiative decay (k_R) and non-radiative decay (k_{NR}) were determined to be 1.46×10^7 and 1.49×10^7 s⁻¹, respectively. The intersystem crossing rate constant for the transition between S_1 and T_1 (k_{ISC}) is 4.47×10^7 s⁻¹, while the reverse intersystem crossing rate constant (k_{RISC}) for the transition from the T_1 level to S_1 level is 5.53×10^4 s⁻¹, a value that is faster than that of **t-DABNA** (2.15×10^4 s⁻¹ as a 3 wt% doped films in mCBP¹⁰). A summary of photophysical data is provided in Table 1.



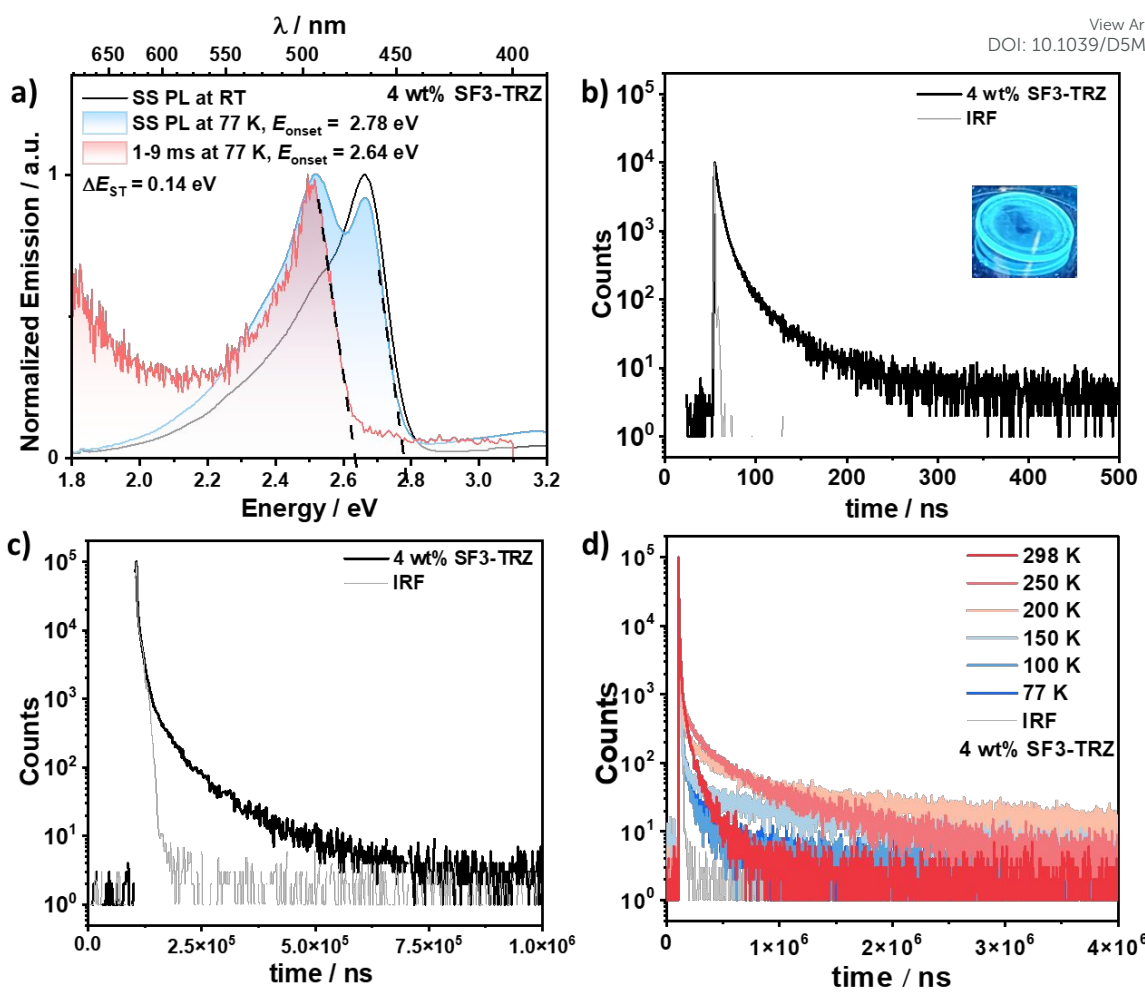


Figure 4. Photophysical data of the 4 wt% doped film of **Mes-tDABNA** in SF3-TRZ; (a) steady-state PL spectra at room temperature (black) and 77 K (blue) and time-gated emission spectrum (1-9 ms) at 77 K (red) (λ_{exc} = 340 nm); (b) Time-resolved PL decay under vacuum measured by TCSPC (λ_{exc} = 375 nm); (c) Time-resolved PL decay under vacuum measured by MCS (λ_{exc} = 375 nm); (d) temperature-dependent time-resolved PL decay (λ_{exc} = 375 nm).

Table 1. Photophysical data of **Mes-tDABNA** in dilute solution and doped film.

Compo und	$\lambda_{\text{Abs}}(\epsilon)$ ^a	λ_{PL} _{a,b}	FW	$E_{\text{SI}}^{c,d}$ / eV	$E_{\text{T1}}^{e,f}$ / eV	ΔE_{ST}^g / eV	Φ_{PL} _{h,i} / %	$\tau_{\text{p,avg}}^j$ /ns	$\tau_{\text{d,avg}}^k$ /μs	k_{ISC}^l / $\times 10^7$ s ⁻¹	k_{RISC}^l / $\times 10^4$ s ⁻¹	$k_{\text{s_r}}^l$ / $\times 10^7$ s ⁻¹
	/ nm ($\times 10^3$ M ⁻¹ cm ⁻¹)		HM _{a,b} / nm									
			/ nm	/ nm								
Mes- tDABN A	444 (24)	460/ 464	25/ 39	2.78/ 2.78	2.65/ 2.64	0.13/ 0.14	58/ 75	7.9/13 .4	--/45.2	4.47	5.53	1.49

^a In toluene solution (10⁻⁵ M). ^b Measured as spin-coated thin films consisting of 4 wt% emitter in SF3-TRZ host. λ_{exc} = 340 nm. ^c Onset of steady-state emission at 77 K in 2-MeTHF glass λ_{exc} = 340 nm. ^d Onset of the SS PL at 77 K in 4 wt% doped film in SF3-TRZ. λ_{exc} = 340 nm. ^e Onset of the time-gated PL spectrum (1-9 ms) at 77 K in 2-MeTHF glass. λ_{exc} = 340 nm. ^f Onset of the time-gated PL spectrum (1-9 ms) at 77 K in 4 wt% doped film in SF3-TRZ. λ_{exc} = 340 nm. ^g $\Delta E_{ST} = E(S_1) - E(T_1)$. ^h Absolute Φ_{PL} of the thin films measured using an integrating sphere. λ_{exc} = 340 nm. ⁱ Φ_{PL} in solution was measured by the relative method using quinine sulfate as the reference (Φ_r = 54.6% in 1 N H₂SO₄).²³ ^j Prompt PL lifetimes were measured by TCSPC and fitting the decay to a multiexponential decay function λ_{exc} = 375 nm. ^k Delayed PL lifetimes were measured by MCS and fitting the decay to a multiexponential decay function λ_{exc} = 375 nm. ^l Intersystem and reverse intersystem crossing

rate constants were calculated using the steady-state approximation method as described in the literature.²⁴

View Article Online
DOI: 10.1039/D5MA00586H

Electrochemistry

Cyclic voltammetry (CV) and differential pulse voltammetry (DPV) measurements in degassed dichloromethane (DCM) containing 0.1M [ⁿBu₄N]PF₆ as a supporting electrolyte and Fc/Fc⁺ as the internal reference (0.46 V vs. saturated calomel electrode (SCE)²⁵) were used to determine the HOMO and LUMO energies (Figure S2). The oxidation wave is irreversible, with an E_{ox} of 0.72 V vs SCE. The corresponding HOMO level is -5.07 eV. This is similar to the HOMO levels reported for **3tPAB** (-5.09 eV) and **tDPAC-BN** (-5.10 eV).^{13, 14} No reduction could be detected, indicating a shallow LUMO level. Therefore, the LUMO level was inferred from the E_{ox} and the optical bandgap, itself determined to be 2.74 eV from the intersection of the normalized absorption and emission spectra in dilute toluene solution (Figure S13). The corresponding LUMO level is -2.33 eV, which also aligns with the reported measured values for **3tPAB** (-2.36 eV) and **tDPAC-BN** (-2.37 eV) in DCM.^{13, 14} However there are varying HOMO and LUMO levels for DABNA-based emitters reported in the literature. For **tDABNA**, **M-tDABNA** and **t-DABNA-dtB** the reported HOMO/LUMO level are -5.72/-3.02, -5.70/-3.00 and -5.71/-3.08, respectively.^{9, 10, 15} The origin of this difference remains unclear, given that there are only minor structural differences across these three emitters; a possible explanation for the divergence in HOMO/LUMO values could be the application of different conversion equations to derive the energy levels from experimental data.

OLEDs

We next fabricated vacuum-deposited OLEDs with **Mes-tDABNA** as the emitter using a device structure consisting of indium tin oxide (ITO)/ 1,4,5,8,9,11-hexaazatriphenylenehexacarbonitrile (HATCN, 5 nm)/ 1,1-bis[(di-4-tolylamino)phenyl]cyclohexane (TAPC, 30 nm)/ tris(4-carbazoyl-9-ylphenyl)amine (TCTA, 10 nm)/ mCP (5 nm)/ emitting layer (EML) (20 nm)/ 1,3,5-tris(3-pyridyl-3-phenyl)benzene (TmPyPB, 40 nm)/ lithium fluoride (LiF, 1 nm)/ aluminum (Al, 100 nm). Here, HATCN was used as the hole injection layer, TAPC and TCTA as the hole transporting layers, mCP as an exciton blocking layer, TmPyPB as an electron transporting layer, and LiF was used to reduce the work function of the top Al electrode. The OLED device stack and the chemical structures of the organic layers are shown in Figure 5d.

We first optimized the doping concentration in SF3-TRZ as a function of Φ_{PL} (Figure S6) A doping concentration of 4 wt% provided charge balance and a sufficiently large exciton recombination zone, and the Φ_{PL} remained high at this concentration (*vide supra*) and an EQE_{max} of 18.4% was achieved at this doping concentration. The electroluminescence (EL) spectrum, current density-voltage-luminance (*J-V-L*) curves and EQE vs luminescence curves are shown in Figure 5a-c. The device with **Mes-tDABNA** emitted narrowband blue light at λ_{EL} of 468 nm (FWHM of 32 nm), which corresponds to CIE coordinates of (0.13, 0.15). These are identical to the reported device with **tDABNA** in DPEPO.⁹ Compared to the devices with **t-DABNA-dtB** (λ_{EL} = 471 nm), the λ_{EL} is blue-shifted; however, due to the broader envelope of the EL spectrum of the device with **Mes-tDABNA** the CIE_y coordinate is increased from 0.13 for the device with **t-DABNA-dtB** (FWHM = 140 meV) to 0.15 for the device with **Mes-tDABNA** (FWHM = 190 meV). The EL spectrum is narrower than the corresponding PL spectrum (Figure 4), which is likely due to the more homogeneous film achieved by vacuum deposition compared to the spin-coated film used for the PL measurements. The device with **Mes-tDABNA** showed an EQE_{max} of 18.4 % and a maximum brightness, L_{max} , of 3600 cd m⁻². Due in part to its relatively slow k_{RISC} , the device showed relatively severe efficiency roll-off at high luminance (EQE₁₀₀ and EQE₁₀₀₀ of 12.5 and 5.6%, respectively); however, the efficiency roll-off was nonetheless milder compared to



devices with **DABNA-1** and **tDABNA**, as neither were reported to reach 1000 cd m^{-2} .^{8, 9} The device with **Mes-tDABNA** performed comparably to one of the best devices with the DABNA derivative **DABNA-NP-TB**, which has a reported $\text{EQE}_{\text{max}}/\text{EQE}_{1000}$ of 19.5/12.0% (Figure 6, Table S3).¹²

In a bid to improve the exciton utilization efficiency and reduce the efficiency roll-off, HF OLEDs were fabricated (Figure 5d). **DMAC-DPS** was used as the TADF assistant dopant because of its high Φ_{PL} of 90%, relatively fast k_{RISC} of $2.9 \times 10^5 \text{ s}^{-1}$ in 20 wt% doped SF3-TRZ film, and the strong overlap between the absorption spectrum of **Mes-tDABNA** and the PL spectrum of **DMAC-DPS** in toluene (Figure S13). An optimized doping ratio of 2 wt% **Mes-tDABNA**:20 wt% **DMAC-DPS**:78 wt% SF3-TRZ was identified to be used as the EML as this formulation minimized the probability for triplet excitons from the host to transfer to the **Mes-tDABNA** and permitted an efficient FRET from **DMAC-DPS** to **Mes-tDABNA**, thereby conserving the narrowband emission (Table 2, Figure S10). The photophysical properties of the hyperfluorescent film are compiled in Table S2. As shown in Figure 5b, the HF devices showed similar narrowband emission at λ_{EL} of 469 nm (FWHMs of 34 nm) and CIE coordinates of (0.13, 0.17) to the conventional device. The turn-on voltages (V_{on}) were reduced from 3.9 to 3.1 V and the EQE_{max} was improved to 23.1%. More importantly, the efficiency roll-off was reduced, with EQE_{100} and EQE_{1000} of 20.5 and 12.7%, respectively. Compared to the HF devices with the derivatives **tDPAC-BN** ($\text{EQE}_{\text{max}}/\text{EQE}_{1000} = 21.0/5.4\%$) and **M-tDABNA** ($\text{EQE}_{\text{max}}/\text{EQE}_{1000} = 8.6/8.1\%$), the OLED with **Mes-tDABNA** showed an enhanced performance evidenced by the milder efficiency roll-off (see additional device comparison data in Table S3 in the SI).



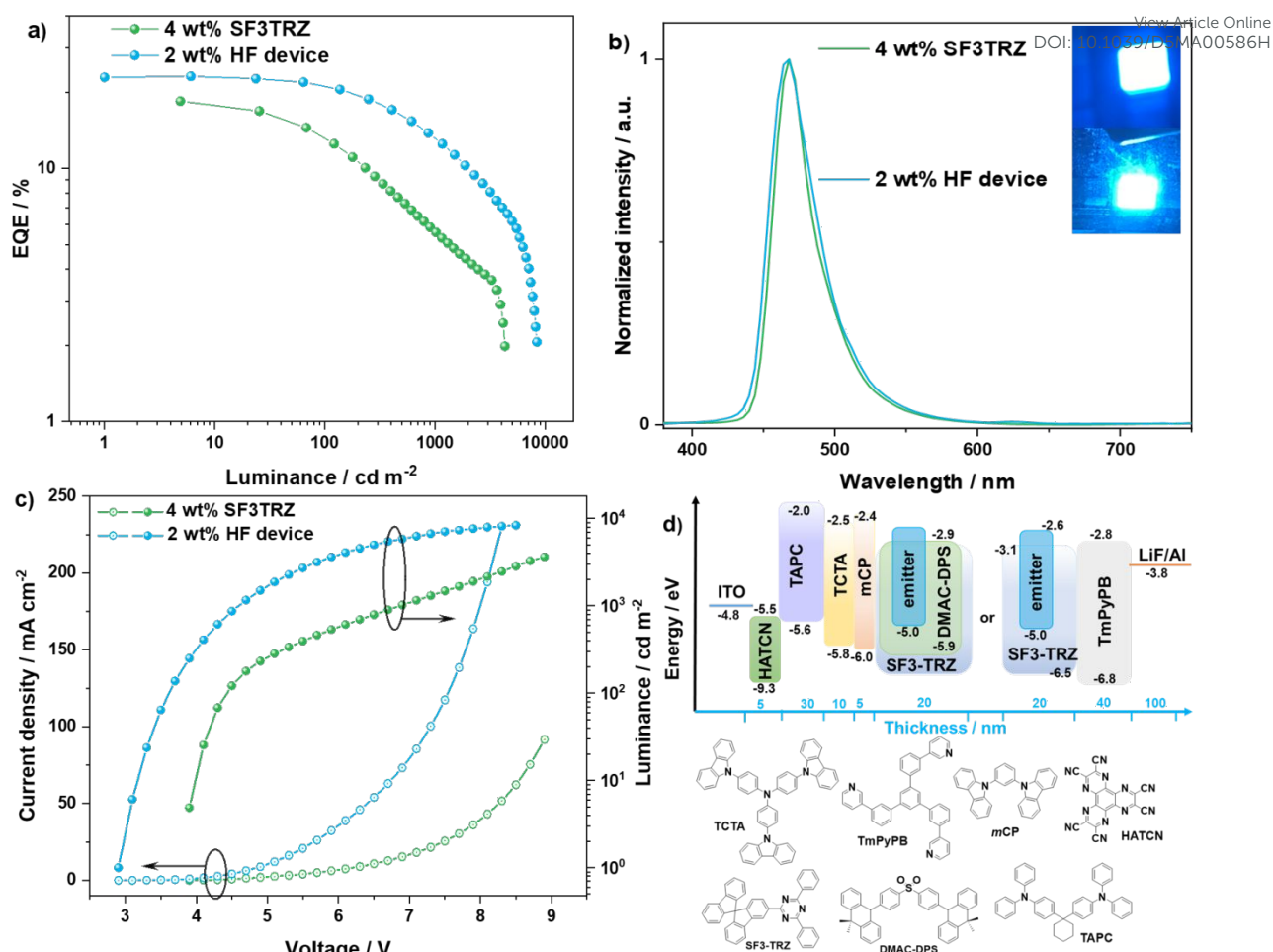


Figure 5. Device data of **Mes-tDABNA** (green = conventional device) (blue = HF device) a) EQE vs Luminance plot; b) electroluminescence spectra; c) J - V - L plot d) device structure and chemical structures of used materials.

Table 2. Device data of **Mes-tDABNA**.

Conventional device ^a	V_{on} / V	λ_{EL}^c (FWHM) / nm	L_{max} / cd m^{-2}	$\text{EQE}_{\text{max}/100/1000}$ / %	CIE (x, y) ^c
Mes-tDABNA (4 wt%)	3.9	468 (33)	3600	18.4/12.5/5.6	0.13,0.15
HF device^b					
Mes-tDABNA (2 wt%)	3.3	469 (34)	8400	23.1/20.5/12.7	0.13,0.17

^a using an EML consisting of 4 wt% **Mes-tDABNA** in SF3-TRZ: ^b using an EML consisting of **Mes-tDABNA**:DMAC-DPS:SF3-TRZ = 2:20:78 wt%.



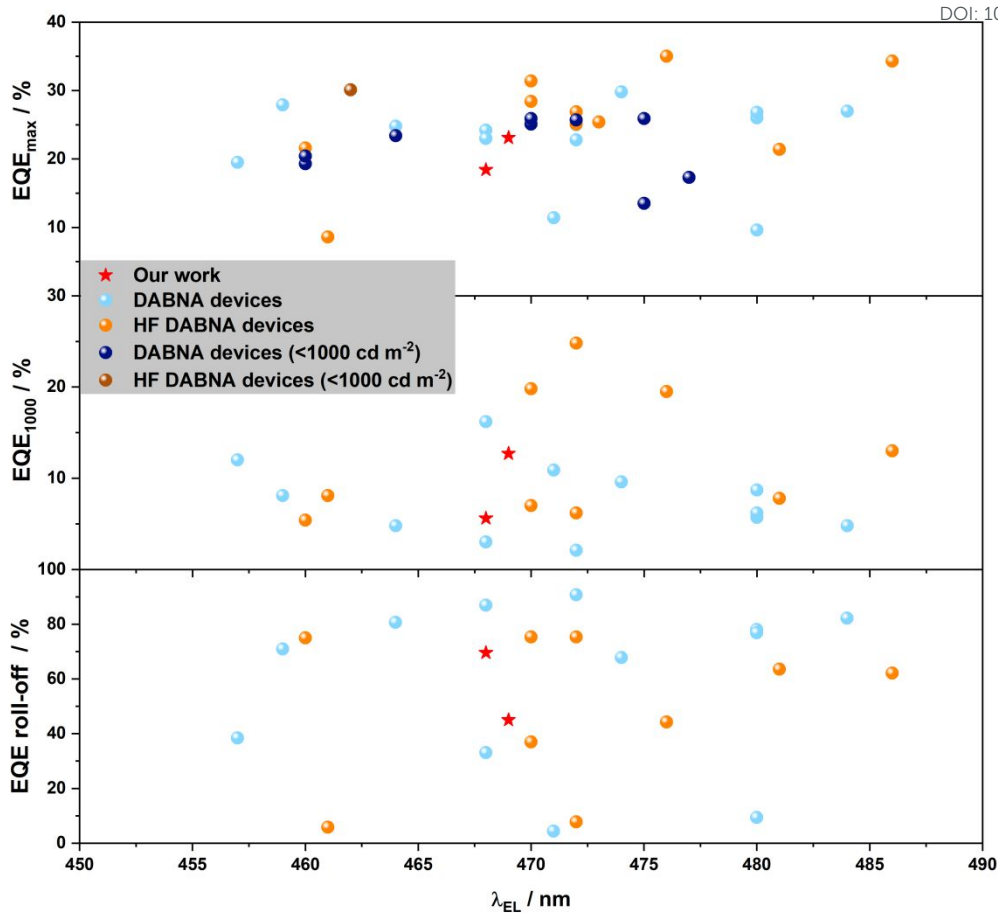


Figure 6. EQE_{max} , EQE_{1000} and EQE roll-off vs λ_{EL} of devices employing DABNA-based emitters in the literature; EQE roll-off refers to the efficiency roll-off from EQE_{max} to EQE_{1000} . Light blue points represent conventional devices; Orange points represent HF devices; Dark blue points represent conventional devices that did not reach a L_{max} of 1000 cd m^{-2} ; brown points represent HF device that did not reach a L_{max} of 1000 cd m^{-2} ; Data presented are listed in Table S2.

Conclusions

Here, we demonstrated an effective substitution strategy to mitigate aggregation-caused quenching in thin films while preserving narrowband blue emission in a DABNA derivative MR-TADF emitter. This approach also resulted in devices showing milder efficiency roll-off and higher EQE_{max} , attributed to a smaller ΔE_{ST} , shorter delayed lifetime, and a faster k_{RISC} , compared to devices with **tDABNA**. **Mes-tDABNA** emits at λ_{PL} at 460 nm and has a narrow emission envelope with a FWHM of 25 nm. The devices showed an EQE_{max} of 18.4% at blue CIE coordinates (0.13, 0.15); however though improved over devices with **tDABNA** there remained a significantly efficiency roll-off (EQE_{1000} of 5.6%, compared to 0.4% for the device with **tDABNA**). To further improve the device performance, the D-A type TADF emitter, **DMAC-DPS**, was employed as a sensitizer within a HF device configuration, resulting in a higher EQE_{max} of 23.1% and lower efficiency roll-off (EQE_{1000} of 12.7%) compared to the traditional device. In contrast, most **tDABNA**-based emitters in HF devices exhibit EQE_{1000} values below 10%. These results underscore the critical role of molecular design in tailoring photophysical properties to enhance device performance.



Supporting Information

View Article Online
DOI: 10.1039/D5MA00586H

^1H NMR and ^{13}C NMR spectra, HRMS, elemental analysis and reverse phase HPLC; supplementary computational data and coordinates; Additional photophysical and OLED data.

Acknowledgments

This project has been partly funded by the European Union Horizon 2021 research and innovation programme under grant agreement No. 101073045 (TADFsolutions) and the EPSRC grant EP/X026175/1. In the UK, this project has received funding from the Engineering and Physical Sciences Research Council for support (EP/R035164/1; EP/W007517/1; EP/Z535291/1). D. Chen thanks the support from China Postdoctoral Science Foundation (Grant No.2022TQ0227) and Natural Science Foundation of Jiangsu Province, China (Grant No. BK20230508). We thank Prof. Xiao-Hong Zhang for providing access to the device fabrication facility at Soochow University.

Data Availability Statement

The research data supporting this publication can be accessed at <https://doi.org/10.17630/e4521ae2-e1ea-45c2-8f60-880c6d12e8a6>.

Author Contributions

M.F.: Conceptualization, Data Curation, Formal Analysis, Investigation, Methodology, Visualization, Writing- Original Draft Preparation, Writing- Review & Editing. D.C.: Data Curation, Formal Analysis, Investigation, Visualization, Writing- Original Draft Preparation, Writing- Review & Editing. E.Z.-C.: Conceptualization, Funding Acquisition, Methodology, Project Administration, Resources, Supervision, Writing – Review & Editing.

References

1. H. Uoyama, K. Goushi, K. Shizu, H. Nomura and C. Adachi, *Nature*, 2012, **492**, 234-238.
2. S. Madayanad Suresh, D. Hall, D. Beljonne, Y. Olivier and E. Zysman - Colman, *Adv. Funct. Mater.*, 2020, **30**.
3. R. K. Konidena and K. R. Naveen, *Adv. Photon. Res.*, 2022, **3**.
4. K. R. Naveen, P. Palanisamy, M. Y. Chae and J. H. Kwon, *ChemComm*, 2023, **59**, 3685-3702.
5. X.-C. Fan, K. Wang, Y.-Z. Shi, Y.-C. Cheng, Y.-T. Lee, J. Yu, X.-K. Chen, C. Adachi and X.-H. Zhang, *Nat. Photonics*, 2023, **17**, 280-285.
6. Y. C. Cheng, X. Tang, K. Wang, X. Xiong, X. C. Fan, S. Luo, R. Walia, Y. Xie, T. Zhang, D. Zhang, J. Yu, X. K. Chen, C. Adachi and X. H. Zhang, *Nat Commun*, 2024, **15**, 731.
7. H. Wang, Y. C. Cheng, X. C. Fan, D. Y. Chen, X. Xiong, X. Y. Hao, Y. Z. Shi, J. Yu, D. Huang, J. X. Chen, K. Wang and X. H. Zhang, *Sci Bull (Beijing)*, 2024, **69**, 2983-2986.
8. T. Hatakeyama, K. Shiren, K. Nakajima, S. Nomura, S. Nakatsuka, K. Kinoshita, J. Ni, Y. Ono and T. Ikuta, *Adv Mater*, 2016, **28**, 2777-2781.
9. S. H. Han, J. H. Jeong, J. W. Yoo and J. Y. Lee, *J. Mater. Chem. C*, 2019, **7**, 3082-3089.
10. J. Park, K. J. Kim, J. Lim, T. Kim and J. Y. Lee, *Adv Mater*, 2022, **34**, e2108581.
11. J. H. Kim, W. J. Chung, J. Kim and J. Y. Lee, *Mater. Today Energy*, 2021, **21**, 100792.
12. S. Oda, W. Kumano, T. Hama, R. Kawasumi, K. Yoshiura and T. Hatakeyama, *Angew Chem Int Ed*, 2021, **60**, 2882-2886.
13. Y. Wang, Y. Duan, R. Guo, S. Ye, K. Di, W. Zhang, S. Zhuang and L. Wang, *Org. Electron.*, 2021, **97**, 106275.



14. Y. Wang, K. Di, Y. Duan, R. Guo, L. Lian, W. Zhang and L. Wang, *Chem. Eng. J.*, 2022, **431**, 133221. View Article Online
DOI: 10.1039/D1SM00586H
15. H. Lim, S. J. Woo, Y. H. Ha, Y. H. Kim and J. J. Kim, *Adv Mater*, 2022, **34**, e2100161.
16. Y. Yuan, X. Tang, X. Y. Du, Y. Hu, Y. J. Yu, Z. Q. Jiang, L. S. Liao and S. T. Lee, *Adv. Opt. Mater.*, 2019, **7**.
17. D. Hall, S. M. Suresh, P. L. dos Santos, E. Duda, S. Bagnich, A. Pershin, P. Rajamalli, D. B. Cordes, A. M. Z. Slawin, D. Beljonne, A. Köhler, I. D. W. Samuel, Y. Olivier and E. Zysman-Colman, *Adv. Opt. Mater.*, 2019, **8**.
18. D. Hall, J. C. Sancho-Garcia, A. Pershin, D. Beljonne, E. Zysman-Colman and Y. Olivier, *J. Phys. Chem. A*, 2023, **127**, 4743-4757.
19. P. Ulukan, A. Monari and S. Catak, *ChemPhotoChem*, 2023, **7**, e202300147.
20. D. Hall, J. C. Sancho-Garcia, A. Pershin, G. Ricci, D. Beljonne, E. Zysman-Colman and Y. Olivier, *J. Chem. Theory Comput.*, 2022, **18**, 4903-4918.
21. L. Hämmerling and E. Zysman-Colman, *Chem Catalysis*, 2024, **4**.
22. L. S. Cui, S. B. Ruan, F. Bencheikh, R. Nagata, L. Zhang, K. Inada, H. Nakanotani, L. S. Liao and C. Adachi, *Nat Commun*, 2017, **8**, 2250.
23. W. H. Melhuish, *J. Phys. Chem.*, 1961, **65**, 229.
24. Y. Tsuchiya, S. Diesing, F. Bencheikh, Y. Wada, P. L. dos Santos, H. Kaji, E. Zysman-Colman, I. D. W. Samuel and C. Adachi, *J. Phys. Chem. A*, 2021, **125**, 8074.
25. V. V. Pavlishchuk and A. W. Addison, *Inorg. Chim. Acta*, 2000, **298**, 97-102.

